PERGAMON

International Journal of Heat and Mass Transfer 43 (2000) 1811–1822

International Journal of HEAT and MASS TRANSFER

www.elsevier.com/locate/ijhmt

Measurements of impinging jet flow and heat transfer on a semi-circular concave surface

Mansoo Choi[a,b,*], Han Seoung Yoo[a], Geunyoung Yang[a,b], Joon Sik Lee[a], Dong Kee Sohn[a,b]

[a]*School of Mechanical and Aerospace Engineering, Seoul National University, Seoul 151-742, South Korea*
[b]*Center for Nano Particle Control, Institute of Advanced Machinery and Design, Seoul National University, Seoul 151-742, South Korea*

Received 15 April 1999; received in revised form 20 July 1999

Abstract

An experimental study of fluid flow and heat transfer has been carried out for jet impingement cooling on a semi-circular concave surface. The distributions of mean velocity and velocity fluctuation on the concave surface have been measured in free, impinging and wall jet flow regions by using a Laser Doppler Anemometer. Local Nusselt numbers have also been measured. Variations of jet Reynolds numbers, the spacing between the nozzle and the target and the distance from the stagnation point in the circumferential direction have been considered. Emphasis has been placed on measuring turbulent jet flow characteristics including impinging and evolving wall jets and interpreting heat transfer data, particularly, the occurrence and its location of secondary peak in connection with data of measured mean velocity and velocity fluctuations on the concave surface.

Keywords: Jet impingement cooling; Concave surface; Impinging jet; Wall jet

1. Introduction

Jet impingement cooling has been widely used for elements exposed to high temperatures and/or high heat flux because of its advantages in effective removal of locally concentrated heat and easy adjustment to the location where cooling is needed. Typically, applications will include paper drying, electronics cooling, annealing of glass. In particular, this jet impingement cooling has been effectively used to eliminate excessive thermal load near the leading edge of gas turbine blade inner surface [1].

Jet impingement cooling with its possible applications, has been extensively studied for many years, and has been well recognized and reviewed [2–4] for single round or slot nozzle and arrays of round or slot nozzles.

When jet impingement cooling is applied to curved surfaces such as the turbine blade surface, the curvature effect should be taken into consideration. For flows on the surface with concave curvature, the centripetal force due to the curvature makes the flow unstable usually and the so-called Taylor–Görtler type vortex is produced [5,6]. Such a vortex has its axis parallel to the flow direction and is known to enhance

* Corresponding author. Tel.: +82-2-880-7128; fax: +82-2-883-0179.
E-mail address: mchoi@plaza.snu.ac.kr (M. Choi).

0017-9310/00/$ - see front matter
PII: S0017-9310(99)00257-4

Nomenclature

A	heating surface area
a	coordinate perpendicular to the concave surface
B	two-dimensional slot jet width
h	convection heat transfer coefficient
H	distance between nozzle exit and stagnation point of target surface
I	electrical current (A)
k	thermal conductivity
Nu_{2B}	Nusselt number ($Nu_{2B} = h2B/k$)
$Nu_{2B,0}$	Nusselt number at stagnation point
Re_{2B}	jet Reynolds number at nozzle exit ($Re_{2B} = U_{avg}2B/\nu$)
q_{loss}	heat loss
q_w	heat flux on the heating surface
s	circumferential distance from the stagnation point
T_j	jet temperature
T_w	wall temperature
U	mean velocity
U_j	jet velocity at the center of the nozzle exit
U_{avg}	area averaged jet velocity at the nozzle exit
u	velocity fluctuation
V	voltage drop
x, y, z	coordinate system

Greek symbols

ν	kinematic viscosity
$\cos\phi$	power factor

momentum and energy transfer and thereby heat transfer rate on the surface. McCormack et al. [7] found that Nusselt numbers on the concave surface of the test duct were increased by 100–150%. Kottke [8] investigated how disturbances superimposed on the mainstream interacted with the Taylor–Görtler vortex for different mesh type, mesh size, mainstream velocity, and the distance between the mesh and test duct front. However, studies of jet impingement cooling on the convexed or concaved surface are not encountered so frequently as those on the flat plate. Chupp et al. [9] and Metzger et al. [10] measured impingement cooling by a row of circular jets on the semi-circular surface and investigated the effects of jet-to-jet spacing and the distance between jet and a cooling surface. Dyban and Mazur [11] measured heat transfer coefficients on the parabolic concave surface and studied the effects of jet-flow passage curvature formed by the cooling surface and the nozzle outer surface. Tabakoff and Clevenger [12] considered impingement cooling on a semi-circular concave surface by a slot jet, a row jet and an array jet to study the cooling effect of various jet-hole arrangements. Metzger et al. [13] studied the heat transfer characteristics according to variations of leading edge shape of the cooling surface and the gap between the leading edge and jet exit. Hsueh and Chin [14] measured mass transfer rate on a convex cylindrical surface impinged by slot jets. Bunker and Metzger [15], Metzger and Bunker [16] suggested that the major influencing parameters were the Reynolds number, leading edge shape, jet spacing and size, jet arrangement, number of jet holes, and the distance between jet exit and leading edge. They also conducted showerhead type cooling experiments and showed that the variation of heat transfer was significant depending on different impinging jet and film hole locations. Gau and Chung [17] visualized the jet flow impinging on both convex and concave semi-circular surfaces and showed the distinctive characteristics of flow and heat transfer on these surfaces. They also showed that as the curvature increased, so did the Nusselt number due to the vigorous vortex motion in the jet mixing region. Lee and Lim [18] considered heat transfer from a convex hemispherical surface impinged by a round impinging jet. Recently, a study of slot jet impingement cooling on concave surface has been done to identify the effects of nozzle shape and curvature (Yang et al. [19]).

Most of the above mentioned studies of jet impingement cooling on curved surfaces mainly focused on heat and/or mass transfer measurements lacking flow data. The turbulent jet flow characteristics should be identified for a clear understanding of heat transfer phenomena and, in particular, wall jet flows as well as impinging jet flows need to be measured to explain measured heat transfer characteristics correctly. Measurements of turbulent impinging jet flows have been done mainly on the flat plate [20,21]. However, measurements of turbulent impinging jet flows on the curved surface are rarely found. The intent of the present study is to provide quantitative measurement data of the turbulent jet flows on the semi-circular concave surface including impinging and wall jets. Jet impingement heat transfer on the curved surface has also been measured and its characteristics has been interpreted using measured impinging and wall jet flows. The present turbulent jet flow data can also serve as bench-marking data for turbulence modeling of jet impingement on curved surfaces.

2. Experimental apparatus and procedure

Turbulent jet flows and heat transfer have been measured separately since forced convection is the dominant heat transfer mechanism. The experimental set-up for heat transfer measurement is depicted in Fig. 1. The air jet was supplied by a compressor through the orifice flow meter and the settling chamber. An air dryer and a filter were attached on the compressed air line to remove water mist, oil drops and dust. A pressure regulator and a needle valve were installed to control the flow rate. The settling chamber with meshes provides uniform and low turbulence intensity at the nozzle exit. Note that the target of impingement has the semi-circular concave surface with 150 mm diameter. The temperature difference between the jet at nozzle exit and the ambient air was within $\pm 0.5^{\circ}C$. Spray atomizer has been installed in the settling chamber to provide seed particles for LDV measurements of turbulent flows.

During the measurement of heat transfer coefficients, the surface was directly heated by applying an electric current through the stainless steel foil of thickness 30 μm. This system can provide the constant heat flux boundary condition on the test surface. Since the resistivity of the stainless steel foil is very small ($\sim 70 \times 10^{-8}\ \Omega$ m), the two stage transformers have been utilized to produce low voltage with high electrical current. The heat flux on the surface was controlled by changing output voltage and determined by measuring the electrical current (I) and the power factor ($\cos\phi$) and the voltage drop (V) between the voltage taps soldered on the heated foil.

The concave surface was made by cutting a circular

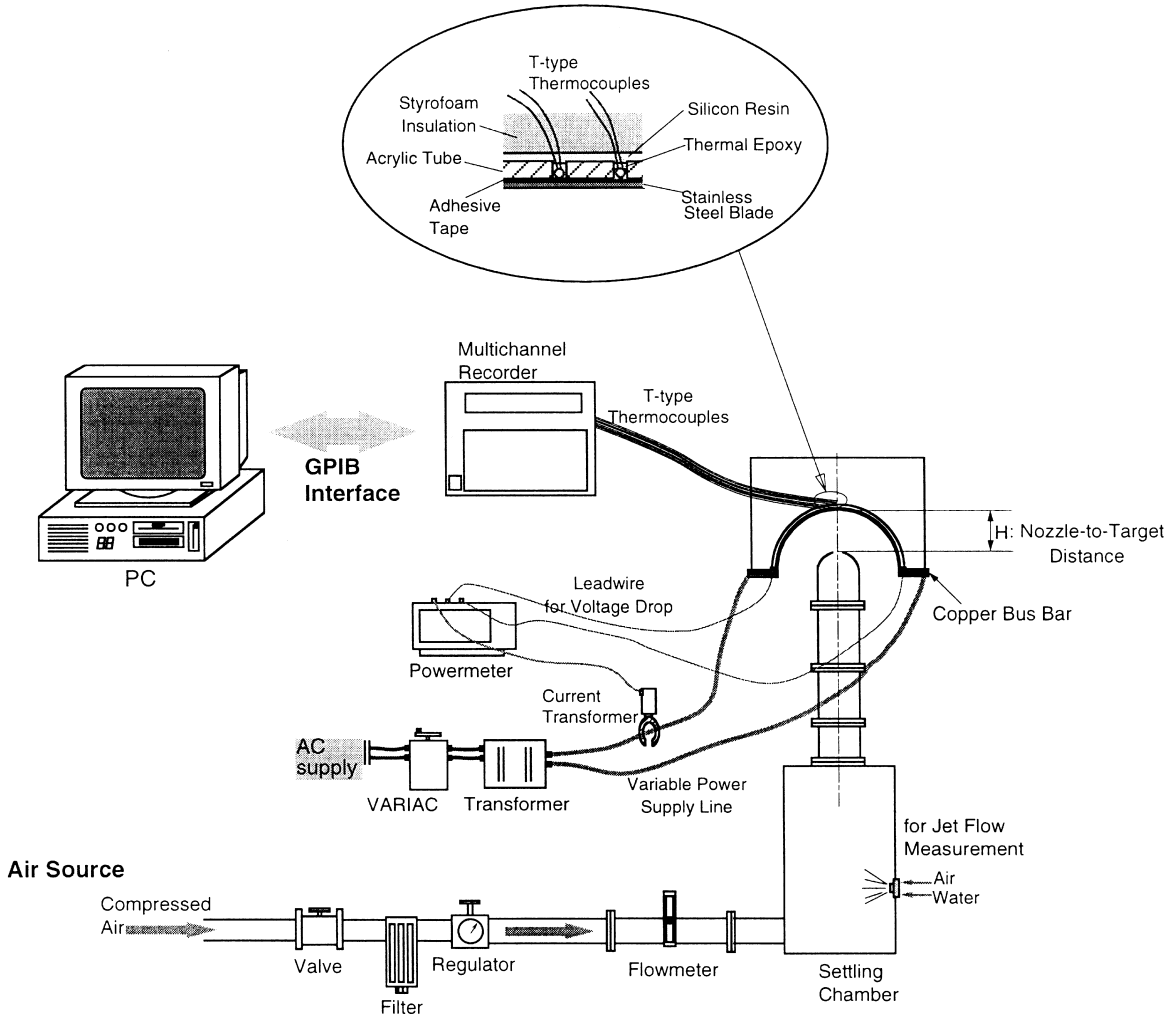

Fig. 1. Experimental apparatus for heat transfer measurements.

acrylic tube and the stainless steel foil was attached to the inner surface with double sided adhesive tape. Thermocouples were installed from an outer acrylic wall by drilling holes and the void space was completely filled with thermal epoxy. The exterior of the target was insulated with Styrofoam to reduce the conductive heat loss through the back surface. Surface temperatures along the concave surface have been measured by T-type thermocouples with 0.01 in. diameter. Thermocouples were installed at 19 locations along the circumferential direction with 5–10 mm separation. The measured temperature data were recorded by a multi-channel recorder and transferred to the personal computer through the GPIB interface.

Fig. 2 shows the experimental set-up for measuring turbulent flows of free, impinging and wall jets. One component back scattering type Laser Doppler Anemometer (LDA, Macrodyne) measures the mean velocity and velocity fluctuation distributions. The signal from LDA was processed by FFT (Fast Fourier Transform) analyzer and transferred to the personal computer for further processing. The laser source for LDA is a 632.8 nm, 10 mW He–Ne laser. The frequency shift was made by a Bragg cell. The mean velocity and the velocity fluctuation at the local point were obtained from collecting more than 5000 data. The seeding particles generated by a spray atomizer were supplied in the settling chamber. Salt-water solution was used as

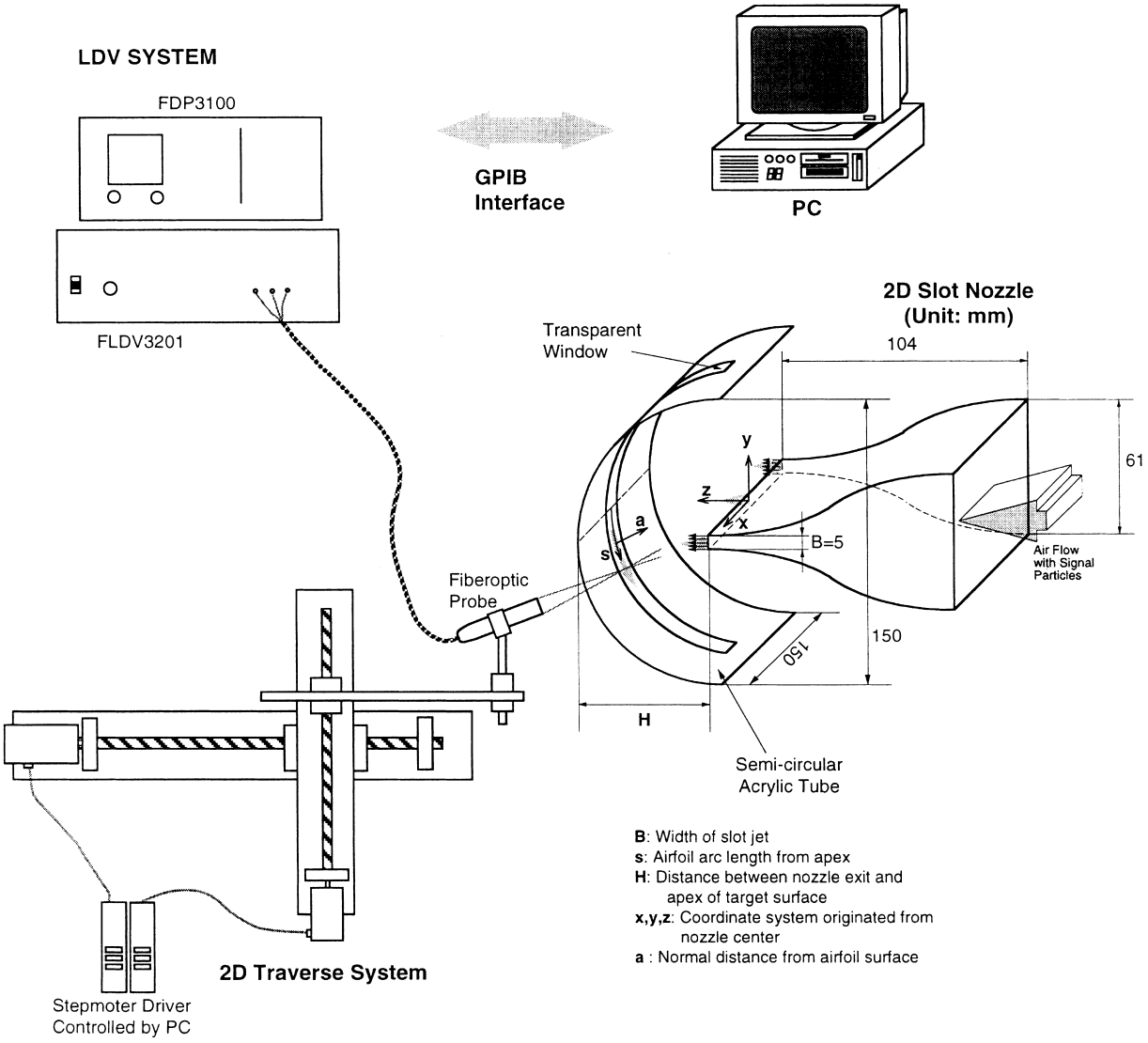

Fig. 2. Experimental apparatus for flow measurements.

an atomizing fluid. The atomizer evaporated the water leaving micron-sized salt particles. A thin transparent window was prepared on the acrylic wall, covered with a transparent thin film of 50 μm thickness, to measure mean velocities and velocity fluctuations from the opposite side of the jet. To accurately position the measuring volume, the computer controlled two-dimensional traverse system was used. Nozzle used in the study was manufactured by following the contour design suggested by Morel [22]; two-dimensional slot nozzle with 5 mm width and the shrinkage ratio of 12.2 : 1 (see Fig. 2).

Jet Reynolds number and RMS value of velocity fluctuation are the two important parameters considered in the present study. The jet Reynolds number and velocity fluctuation (Tu) are defined as follows:

$$Re_{2B} = \frac{U_{\text{avg}} 2B}{\nu} \tag{1a}$$

$$Tu\,(\%) = \frac{\sqrt{\overline{u^2}}}{U_{\text{j}}} \times 100 \tag{1b}$$

where U_{avg} is the area averaged velocity at the nozzle exit, $2B$ is the hydraulic diameter of the two-dimensional slot jet, and u is the velocity fluctuation.

The Nusselt number is calculated by

$$Nu_{2B} = \frac{h2B}{k} = \frac{q_{\text{w}}}{T_{\text{w}} - T_{\text{j}}} \frac{2B}{k} \tag{2}$$

The air jet temperature is measured at the settling chamber in order to avoid disturbing the flow field at the nozzle exit. The temperature fluctuation due to the ambient air entrainment is minimized by maintaining the temperature difference between the jet and the ambient air within ± 0.5°C. The heat flux on the wall can be evaluated as described below:

$$q_{\text{w}} = q_{\text{g}} - q_{\text{loss}} = \frac{VI\cos\phi}{A} - q_{\text{loss}} \tag{3}$$

where q_{loss} is the sum of heat losses. Heat losses include conduction through the insulating materials, the lead wires of thermocouples, the stainless steel foil and radiation loss. Total heat loss is estimated to be less than 3.2% of the generated heat flux, q_{g}, therefore, neglected. The uncertainty analysis was performed with 95% confidence level for the measured values by applying the methods suggested by Kline and McClintock [23]. For given experimental conditions, the uncertainties of heat transfer coefficient, Nusselt number and Reynolds number are 6.89, 7.94 and 3.45%, respectively. Measurements of local Nusselt numbers along the semi-circular concave surface using the same nozzle and experimental apparatus has been done before and found to be in a reasonable agreement with the data of Gau and Chung [17,19]. More emphasis in the present study has been placed on measuring turbulent jet flow characteristics.

3. Results and discussion

Fig. 3 shows the evolution of the distributions of axial mean velocity and velocity fluctuation for a free jet at $Re_{2B} = 4740$. Along the streamwise direction, the jet expands. The jet core region remains up to z/B equal to 6 approximately. The values of z/B on the upper parallel coordinate in Fig. 3 designate the origin for the results for each z/B; for example, the line for $z/B = 4$ is the origin for the mean velocity and velocity fluctuation distributions for $z/B = 4$. Near the nozzle exit, the velocity fluctuations were very low near the center of the nozzle but at the edge of the nozzle, the values suddenly became high due to the mixing of the jet and the ambient air. As the mixing layer expands along the streamwise direction, the high turbulence region moves toward the jet center line and the maximum velocity fluctuation exists at the jet center line beyond $z/B = 5$–6. Around the edge of the jet, the distortion on the profile of the turbulence intensity would be observed after $z/D = 4.6$, which could be caused by flow entrainment.

Impinging jet flows along the centerline have been measured for three different Reynolds numbers equal to 1780, 2960 and 4740 as shown in Figs. 4 and 5. In the figures, results for free jets were also included for comparison. As the jet Reynolds number increases, the center line velocity of a free jet drops at the earlier axial locations. The mixing of the jet and the ambient air can be enhanced for higher Reynolds numbers and as a result, the effect of mixing can penetrate up to the center line at the earlier axial location, which reduces the mean velocity at the center and increases turbulence intensity. The region where the center line velocity remains almost constant is known as potential core. The potential core length can be defined as the length of the region where the local velocity is maintained at not less than 95% of the jet velocity at the nozzle exit [3]. The present study resulted in the potential core lengths equal approximately to $8B$ at $Re_{2B} =$ 1780 and 2960 and $5.5B$ at $Re_{2B} = 4740$. Impinging jet flows were measured for three different (nozzle to concave target) spacings of H/B equal to 4, 6 and 10; the target is inside the potential core ($H/B = 4$), near the end of the potential core ($H/B = 6$), and outside the potential core ($H/B = 10$). Impinging jet flows basically follow the trend of free jets initially and deviate from the results of free jets at certain axial locations.

Stagnation region thickness can be defined as the thickness of the region where the velocity profile deviates from the free jet results. It is shown in Fig. 4 that

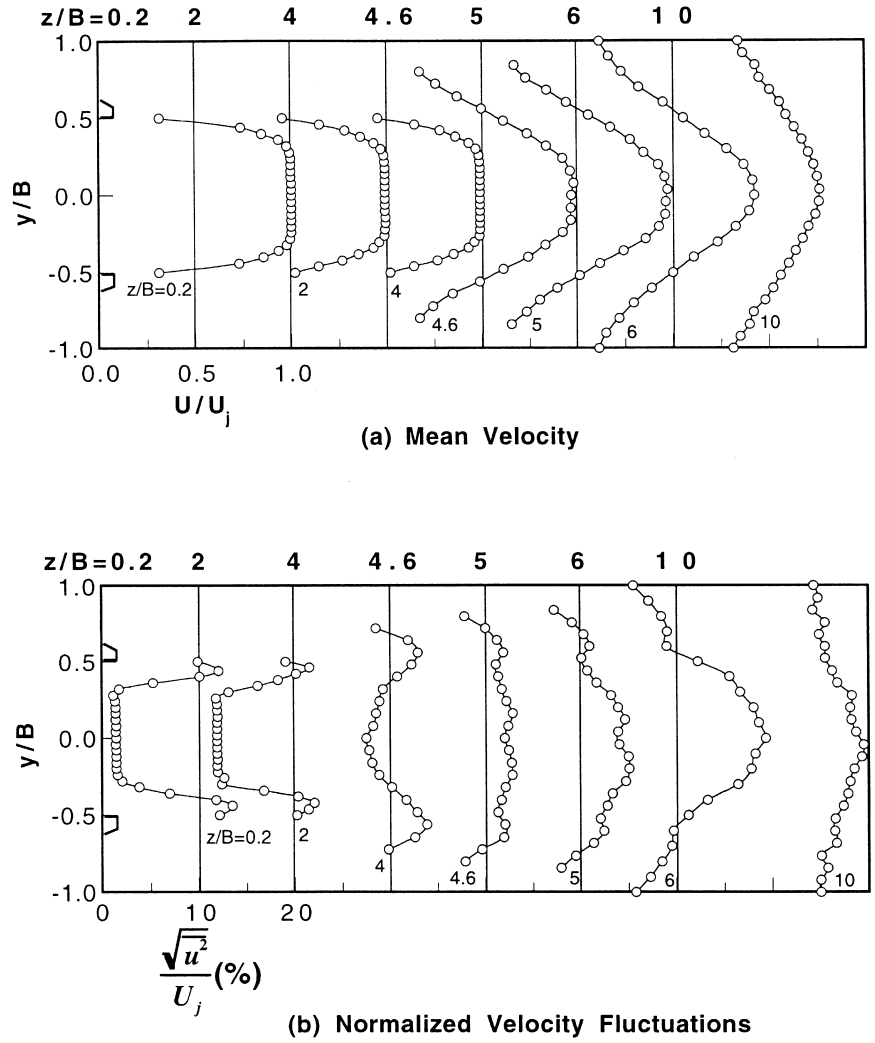

Fig. 3. Evolution of the distributions of axial velocity and velocity fluctuation at $Re_{2B} = 4740$ of a free jet.

the stagnation region thickness is approximately equal to $2B$.

The distributions of velocity fluctuation along the centerline are also shown in Fig. 5. When the target wall is inside the potential core region ($H/B = 4$), velocity fluctuations become higher than those of free jets for all Reynolds numbers considered, which would be mainly due to the sudden drop of streamwise velocity in the stagnation region and its resulting mixing effect while flows for free jets are within the potential core. When the target wall is located outside the potential core ($H/B = 10$), it seems the concave curvature makes the flow entrainment difficult, consequently reducing the turbulence level compared with the results of free jets.

Fig. 6 shows stagnation Nusselt numbers as a function of the impinging distance normalized by the nozzle width (H/B) for three different Reynolds numbers. The variation of stagnation Nusselt numbers can be divided into three different parts as H/B increases: (1) first decreasing part; (2) increasing part; and (3) second decreasing part. For all Reynolds numbers considered, the highest heat transfer rates at the stagnation point occur at the smallest spacing ($H/B = 0.2$). This behavior can be explained by considering the stagnation region thickness. As mentioned earlier, stagnation region thickness is shown to be approximately equal to $2B$ when the target plate is inside the potential core. If the nozzle is placed closer to the target surface than this thickness, the stagnation region thickness should be proportionally reduced to the spacing between the nozzle and the target; consequently, the thermal boundary layer becomes thinner, and heat transfer rates should be increased.

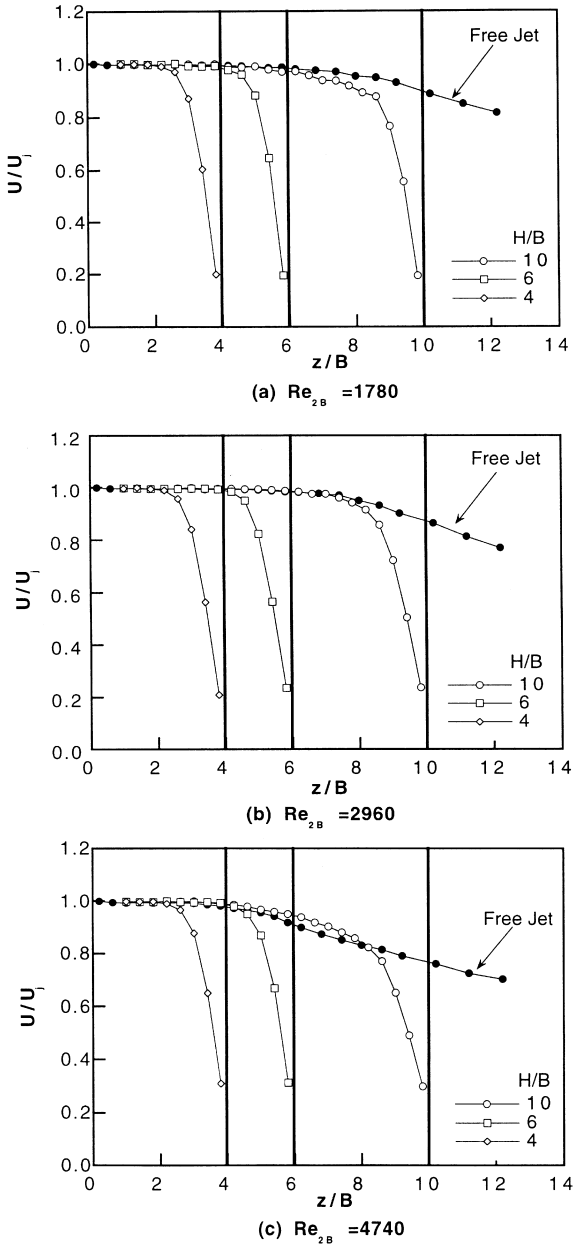

Fig. 4. Axial mean velocity profile along the centerline for free and impinging jet flows.

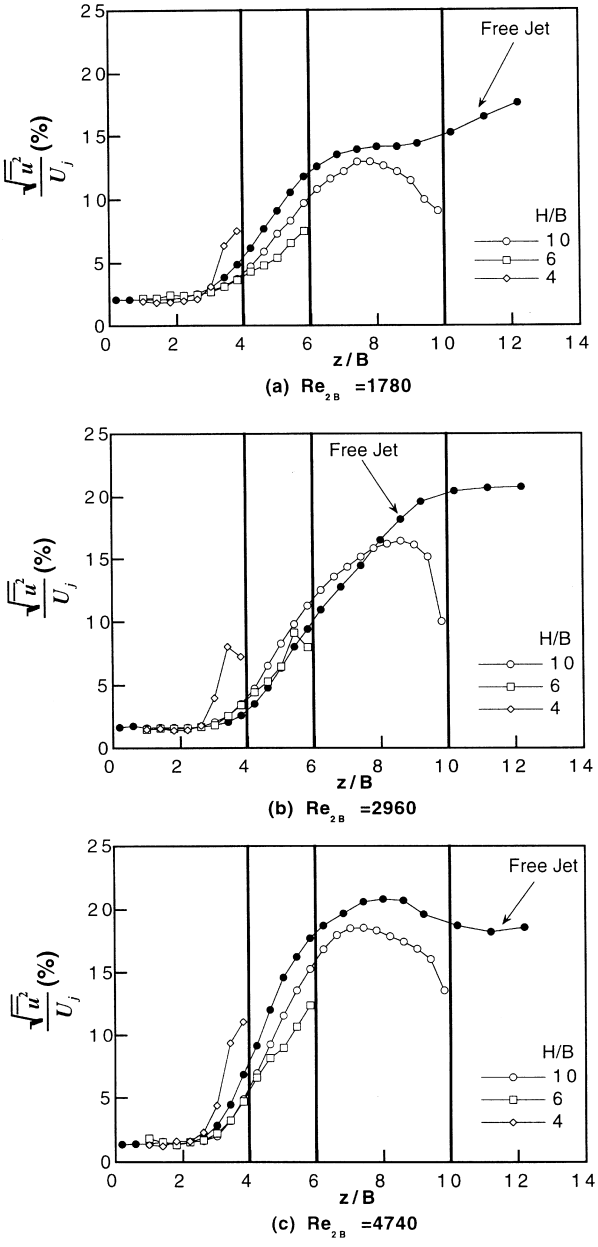

Fig. 5. Normalized velocity fluctuations along the centerline for free and impinging jet flows.

In the second part, the target wall is still located within the potential core region, while the spacing is larger than the stagnation thickness ($2–3 < H/B < 5–6$). In this part, mean velocity of a jet does not vary and the variation of impinging jet mean velocity also does not vary significantly for different spacings as shown in Fig. 4. However, as shown in Fig. 5, the turbulence level for free and impinging jets increases significantly in this part and the turbulence intensities near the target surface for $H/B = 4$ become higher than those of free jets. These substantial increases of turbulence intensity should be the cause to increase heat transfer rates after reaching the minimum as H/B increases as can be seen in Fig. 6. Various studies reported that the heat transfer augmentation was obtained at high turbulence level [24]. The peak of the stagnation Nusselt number occurs at the spacing which is approximately equal to the potential core length.

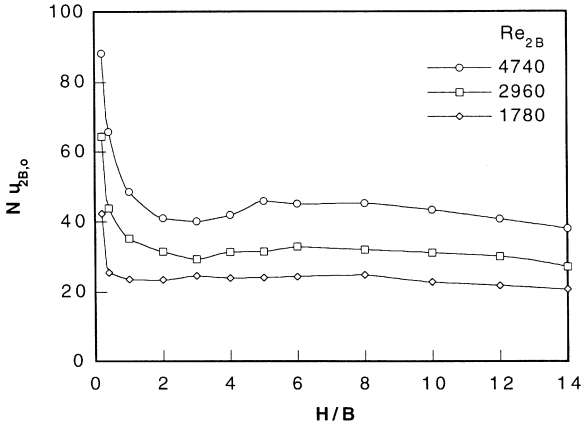

Fig. 6. Variations of stagnation point Nusselt numbers for different H/Bs.

Beyond this spacing, Nusselt numbers again decrease as the spacing increases. In this part, mean velocities decrease significantly although velocity fluctuations remain high. The decrease of mean velocity would be the main reason to lower heat transfer rates on the stagnation point in this part.

Fig. 7 shows the distributions of local Nusselt numbers along the streamwise direction for twelve different spacings at $Re_{2B} = 4740$. As shown in Fig. 7(a), Nusselt number distributions have secondary peaks near $s/B = 4$–5 when the normalized spacing between the nozzle and the target is less than one. When the normalized spacings are larger than one for $Re_{2B} = 4740$, the secondary peaks disappear as shown in Fig. 7(b) and (c). The phenomenon of secondary peaks for impinging jet heat transfer has been extensively studied by many researchers. Gardon and Akfirat [25] explained the secondary peak to be a result of the laminar-turbulence transition of the wall jet, from a flat plate impinging study. Den Ouden and Hoogendoorn [26] suggested that the location of the secondary peak coincided with the point where the product of the boundary layer velocity and the turbulent kinetic energy became the maximum. Kataoka et al. [27] made an effort to explain the secondary peak in connection with the turbulent boundary layer eddy structure of wall jets. Many studies reported that the secondary peak disappeared when the target walls were placed outside the potential core region.

Measurements of local Nusselt numbers have also been made for different Reynolds numbers at two fixed spacings; $H/B = 0.2$ and 0.4. As shown in Fig. 8, the secondary peak occurs closer to the stagnation point as the Reynolds number increases. For different Reynolds numbers of 2960, 4740 and 7100, the secondary peaks occur at $s/B = 6$, 4, 3, respectively, for the case

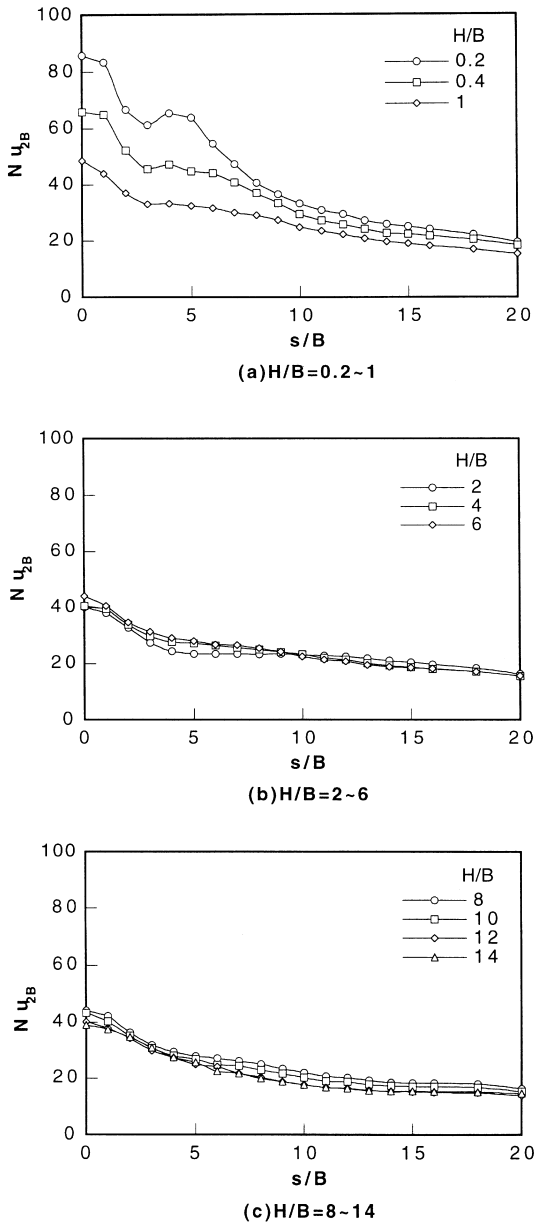

Fig. 7. Distribution of local Nusselt numbers in the circumferential direction at $Re_{2B} = 4740$.

of $H/B = 0.2$. For $H/B = 0.4$, the secondary peak appears for $Re_{2B} = 4740$, but the secondary peak is less pronounced than for $H/B = 0.2$. For $Re_{2B} = 2960$, the decreasing trend of heat transfer rate from the stagnation point turns into a somewhat flat pattern around $s/B = 5$.

Measurements of wall jet flows have been done to explain the variations of local heat transfer rate in the circumferential direction. In the present study, mean velocities and velocity fluctuations of wall jets have

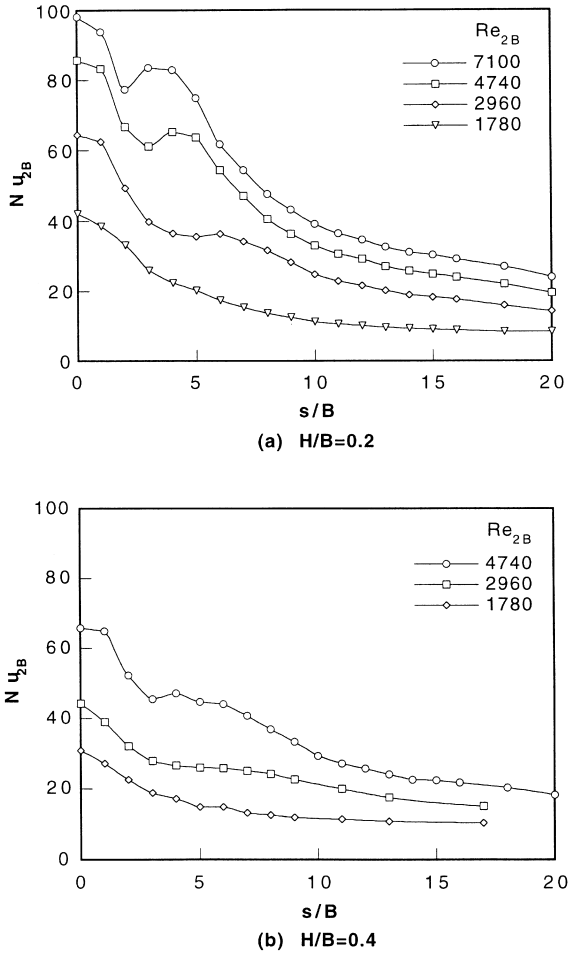

Fig. 8. Variations of local Nusselt numbers in the circumferential direction.

been measured using LDA for three different Reynolds numbers of 1780, 2960 and 4740. Fig. 9 shows the distributions of the circumferential component of the mean velocity for different H/B's at $Re_{2B} = 2960$. The values of s/B on the upper parallel coordinate in Fig. 9 designate the origin of the results for each s/B; for example, the line for $s/B = 4$ is the origin for the mean velocity distribution for $s/B = 4$ where U/U_j is equal to zero. For the case of $H/B = 0.4$ (Fig. 9(a)), the effect of fluid acceleration is clearly observed; mean velocities may exceed nozzle exit velocity up to the region of $s/B = 6$. At $s/B = 6$, the peak velocity occurs near $a/B = 0.45$ and at $s/B = 3$ and 4, there should be peak values at the locations closer to the surface even though measurements have not been successful for the region very near the surface. Fig. 9(a) shows clearly the evolution of the wall jet and it is obvious that the wall jet becomes thickened along the streamwise direction. The evolution of the wall jet can also be seen for different H/B's (Fig. 7(b) and (c)). But, for spacings larger than B (Fig. 9(b)–(d)), the effect of fluid acceleration has not been observed, therefore, all the measured mean velocities have been less than the nozzle exit velocity. For circular jet cases, the velocity excess can occur when the spacings are less than 0.25 times the nozzle diameter [16]. For the present slot nozzle case the velocity excess can be estimated to occur at $H/B < 0.5$ from mass conservation consideration. It is also noted that the thickness of the wall jet is smaller for $H/B = 0.4$ than for $H/B = 1$ and this thinner thickness of the wall jet causes the heat transfer rates for $H/B = 0.4$ to become larger than for $H/B = 1$ as shown in Fig. 7.

The velocity fluctuation distributions measured along the normal direction from the target surface at $H/B = 0.4$ are shown in Fig. 10 for different s/B's and different Reynolds numbers. As the Reynolds number increases, velocity fluctuations also increase; for example, the maximum value of velocity fluctuations is approximately equal to 28% near $s/B = 6$ for $Re_{2B} = 2960$ and 33% near $s/B = 4$ for $Re_{2B} = 4740$ while velocity fluctuations for $Re_{2B} = 1780$ are mostly less than 10%. As mentioned in Fig. 8, location of the secondary peak moves toward the stagnation point as Reynolds number increases. This trend is similar to that of velocity fluctuations. The steep increase of velocity fluctuation near $s/B = 4$ for $Re_{2B} = 4740$ coincides with the increase of heat transfer rate near $s/B = 4$ and the occurrence of the secondary peak near $s/B = 4$–5 as shown in Fig. 8(b). For $Re_{2B} = 2960$, the steep increase of velocity fluctuation can also be observed near $s/B = 6$. This increase also coincides with the variation of heat transfer rate along the circumferential direction; the decreasing trend of heat transfer rate from the stagnation point turns into a somewhat flat pattern around $s/B = 5$ (see Fig. 8(b)).

4. Conclusions

Measurements of impinging jet flows and heat transfer rate on a semi-circular concave surface have been made. Particular emphasis has been placed on turbulent jet flow characteristics including impinging and evolving wall jets and interpreting heat transfer data, particularly, the occurrence and location of secondary peaks in connection with data of measured mean velocity and velocity fluctuations on the concave surface. The following conclusions have been drawn.

1. The potential core length becomes shorter for $Re_{2B} = 4740$ than for $Re_{2B} = 1780$ and 2960. Stagnation region thicknesses are approximately equal to $2B$.
2. For the case of $H/B = 0.4$, the effect of fluid acceleration has been observed. The evolution of wall

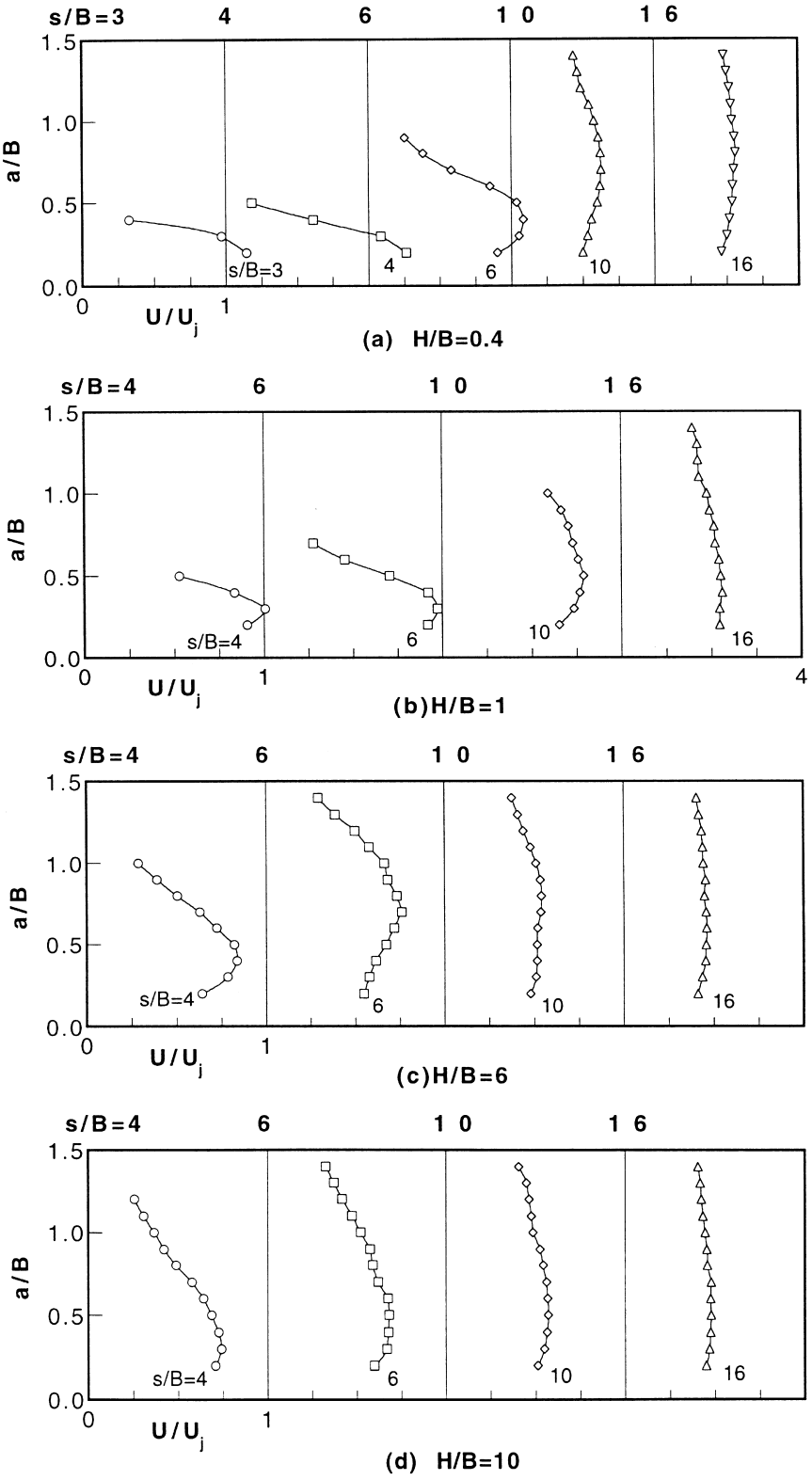

Fig. 9. Mean velocity variations of wall jet flow along the concave surface at $Re_{2B} = 2960$.

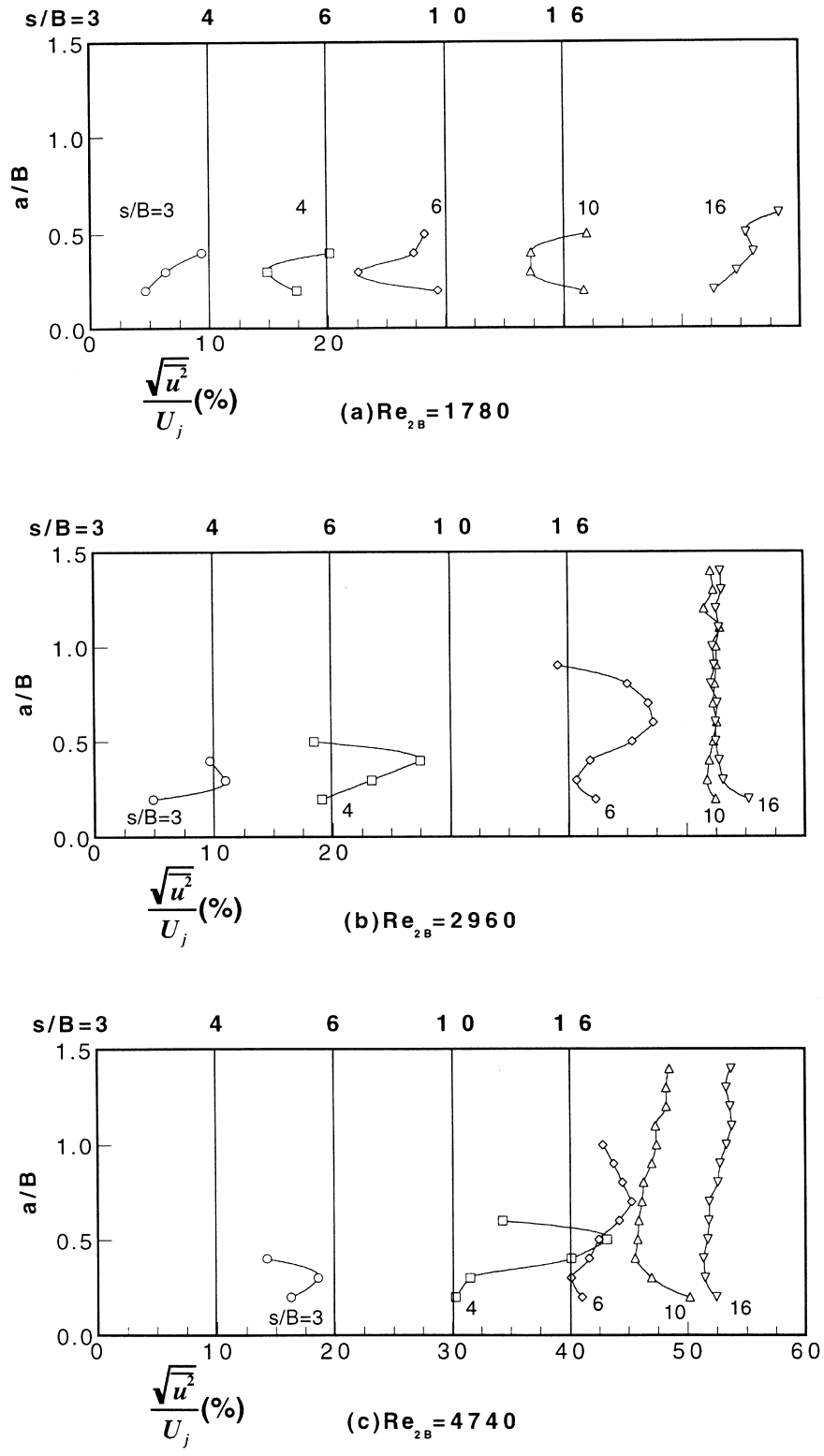

Fig. 10. Normalized velocity fluctuations of wall jet flow along the concave surface for three Reynolds numbers at $H/B = 0.4$.

jets has been successfully measured using a Laser Doppler Velocimeter. The thickness of the wall jet is smaller for $H/B = 0.4$ than for $H/B = 1$, which is the reason why the heat transfer rate for $H/B = 0.4$ is higher than for $H/B = 1$.

3. The occurrence of secondary peaks and their locations have been explained from the variation of measured velocity fluctuations of the wall jets evolving along the streamwise direction.
4. The increase of stagnation heat transfer rate for $2–3 < H/B < 5–6$ has been successfully explained due to the steep increase of velocity fluctuations measured in free and impinging jets.

Acknowledgements

This work was supported by Turbo and Power Machinery Research Center, Korea Science and Engineering Foundation. The support from National CRI Center for Nano Particle Control which is designated by the Ministry of Science and Technology, Republic of Korea is also gratefully acknowledged.

References

[1] C.O. Gardon, Aerothermodynamics of Aircraft Engine Components, AIAA Education Series, 1985, pp. 273–328.
[2] H. Martin, Heat and mass transfer between impinging gas jets and solid surface, Advances in Heat Transfer 13 (1977) 1–60.
[3] K. Jambunathan, E. Lai, M.A. Moss, B.L. Button, A review of heat transfer data for single circular jet impingement, Int. J. Heat and Fluid Flow 13 (1992) 106–115.
[4] R. Viskanta, Heat transfer to impinging isothermal gas and flame jets, Experimental Thermal and Fluid Science 6 (1993) 111–134.
[5] H. Thomann, Effect of streamwise wall curvature on heat transfer in a turbulent boundary layer, Journal of Fluid Mechanics 33 (1968) 283–292.
[6] R.E. Mayle, M.F. Blair, F.C. Kopper, Turbulent boundary layer heat transfer on curved surfaces, ASME Journal of Heat Transfer 101 (1981) 521–525.
[7] P.D. McCormack, H. Welker, M. Keeleher, Taylor–Görtler vortices and their effect on heat transfer, ASME J. of Heat Transfer 92 (1970) 101–112.
[8] V. Kottke, Taylor–Görtler vortices and their effect on heat and mass transfer, in: Eighth International Heat Transfer Conference, vol. 3, 1986, pp. 1139–1144.
[9] R.E. Chupp, H.E. Helms, P.W. Mcfadden, T.R. Brown, Evaluation of internal heat transfer coefficients for impingement-cooled turbine airfoils, J. of Aircraft 6 (1969) 203–208.
[10] Y.P. Dyban, A.I. Mazur, Heat transfer from a flat air jet flowing into a concave surface, Heat Transfer — Soviet Research 2 (1970) 15–20.
[11] D.E. Metzger, T. Yamashita, C.W. Jenkins, Impingement cooling of concave surfaces with lines of circular air jets, ASME J. of Engineering for Power 91 (1969) 149–158.
[12] W. Tabakoff, W. Clevenger, Gas turbine blade heat transfer augmentation by impingement of air jets having various configurations, ASME J. of Engineering for Power 94 (1972) 51–60.
[13] D.E. Metzger, R.T. Baltzer, C.W. Jenkins, Impingement cooling performance in gas turbine airfoils including effects of leading edge sharpness, ASME J. of Engineering for Power 94 (1972) 219–225.
[14] K.L. Hsueh, D.T. Chin, Mass transfer of a submerged jet impinging on a cylindrical surface, J. of Electrochemical Society 133 (1986) 1845–1850.
[15] R.S. Bunker, D.E. Metzger, Local heat transfer in internally cooled turbine airfoil leading edge regions. Part I: impingement cooling without film coolant extraction, ASME J. of Turbomachinery 12 (1990) 451–458.
[16] D.E. Metzger, R.S. Bunker, Local heat transfer in internally cooled turbine airfoil leading edge regions. Part II: impingement cooling with film coolant extraction, ASME J. of Turbomachinery 112 (1990) 459–466.
[17] C. Gau, C.M. Chung, Surface curvature effect on slot air-jet impingement cooling flow and heat transfer process, ASME J. of Heat Transfer 113 (1991) 858–864.
[18] D.H. Lee, K.B. Lim, Heat transfer from a convex hemispherical plate to a round impinging jet, in: Advances in Turbulence Research—1995, Postech, Pohang, Korea, 1995, pp. 81–100.
[19] G. Yang, M. Choi, J.S. Lee, An experimental study of slot jet impingement cooling on concave surface: effects of nozzle configuration and curvature, Int. J. Heat Mass Transfer 42 (1999) 2199–2209.
[20] D. Lytle, B.W. Webb, Air jet impingement heat transfer at low nozzle-plate spacings, Int. J. Heat Mass Transfer 37 (1994) 1617–1697.
[21] J.A. Fitzgerald, S.V. Garimella, A study of the flow field of a confined and submerged impinging jet, Int. J. Heat Mass Transfer 41 (1998) 1025–1034.
[22] T. Morel, Design of two-dimensional wind tunnel contractions, Journal of Fluids Engineering 99 (1977) 371–377.
[23] S.J. Kline, F.A. McClintock, Describing uncertainties in single-sample experiments, Mech. Eng 75 (1953) 3–8.
[24] R. Gardon, J.C. Akfirat, The role of turbulence in determining the heat-transfer characteristics of impinging jet, Int. J. Heat Mass Transfer 8 (1965) 1261–1272.
[25] R. Gardon, J.C. Akfirat, Heat transfer characteristics of impinging two-dimensional air jets, ASME J. of Heat Transfer 88 (1966) 101–108.
[26] C. Den Ouden, C.J. Hoogendoorn, Local convective-heat-transfer coefficients for jets impinging on a plate; experiments using a liquid-crystal technique, in: Proc. 5th Int.Heat Transfer Conf., vol. 5, 1974, pp. 293–297.
[27] K. Kataoka, M. Suguro, H. Degawa, K. Marul, I. Mihata, The effect of structure renewal due to large-scale eddies on jet impingement heat transfer, Int. J. Heat Mass Transfer 30 (1987) 559–567.